Artequick® as Inhibitor of ASTM A36 Mild Steel Corrosion through Anodic Sites Dissolution: Computational and Electrochemical Approach

B. U. Ugi*, E. C. Omaliko and M. E. Ikpi

Corrosion and Electrochemical Research Laboratory (CER-Lab), Department of Pure and Applied Chemistry, University of Calabar, P. O. Box 1115, Nigeria
*Corresponding author: ugibenedict@gmail.com

Received 06/09/2022; accepted 06/12/2022
https://doi.org/10.4152/pea.2024420301

Abstract
ATK was investigated to ascertain its IE(%) on ASTM A36 MS corrosion in a HCl medium. This was possible through the use of WL, Td, Tm, PDP, EIS and SEM techniques. It was seen from all experimental results that, through adsorption onto the MS surface, ATK mitigated active corrosion sites. CR was seen to decrease with higher inhibitor Ct from 197.6 to 19.3 $mg/hr^{-1}/cm^2$. IE(%) of ATK, which rose from 50 to 90.2%, with corresponding increased Ct, from 150 to 750 ppm, was better by adding PPQ to it than ATS. An increase in R_{ct}, up from 346 to 1153 Ω/cm^2, and a decrease in i_{corr}, from 312.2 to 64.4 mA, were seen, with higher Ct of ATK, which indicated reduced anodic dissolution and better CI. A mixed type inhibition was deduced from Tafel slopes of PDP results. A physical adsorption mechanism was proposed, while, in Td terms, ATK exhibited a stable and spontaneous reaction.

Keywords: ASTM A36 MS; ATK; ATS; corrosion; computational and electrochemical studies; EIS; PDP; PPQ: SEM.

Introduction•

Corrosion is the deterioration of a material, especially metal, in an unfavorable environment [1]. Generally, corrosion involves the decrease in valuable content of metals or alloy structures, to a point where they can no longer support the applied load. Corrosion is usually influenced by water and O, and could be either electrochemical or chemical [1, 2]. The main factor in any corrosion process is the environment, which is complex and susceptible to change over time and prevailing conditions. Metals are majorly used in industry, and installation costs are high, but corrosion decreases their life span. The struggle to hinder corrosion effects on metallic materials has advanced greatly with the use of different protective measures, especially environmental modifications, metals selection and surface conditions [2, 3]. The prompt availability, Pc presence (N, S and P) and low cost of organic CI (plants) has motivated literature to continually research them and verify their properties [3-4]. Similar assertion has been provided by [5], in their

• The abbreviations and symbols definition lists are in pages 167-168.

experimental and quantum chemical studies on tizanidine CI of E24 CS in oil field acidizing solutions. Among the various methods to avert or prevent metal surfaces destruction or degradation, CI are one of the best-known and successful methods of protection [4, 6]. Organic CI enable the formation of a protective film through their Pc atoms adsorption onto a metal surface. CI adsorption displaces water from the metal surface and protects it against deterioration, as previously reported by [6]. Inhibitors can slow corrosion processes, through an increase in β_a or β_c polarization, which originates chemical reaction products on a galvanic/voltaic cell in the electrodes vicinity. This decreases ions movement or diffusion towards the metallic surface, which increases its resistance to current flow and electricity, and frequently reduces the cell EMF [5-7]. Surface chemistry generally defines adsorption as the attraction and retention of molecules in a solid or liquid, which results in higher Ct of molecular species at their surface than in their core [8-10].

ATS molecular formula, molar mass, density and IUPAC name are $_{15}H_{22}O_5$, 282.332 g/mol, 1.24 g/cm^3 and (3R,5aS,6R,8aS,9R,12S,12aR)-octahydro-3,6,9-trimethyl-3,12-epoxy-12H-pyrano[4,3-j]-1,2-benzodioxepin-10(3H)-one, respectively. ATS structure is shown in Fig. 1 [11-13]. PPQ is available as a base and as a water-soluble tetraphosphate salt. Its chemical formula, molecular mass and IUPAC nomenclature are $C_{29}H_{32}Cl_2N_6$, 535.51 g/mol and 1,3-bis[4-(7-chloroquinolin-4-yl) piperazin-1-yl] propane, respectively. PPQ is a white to pale yellow crystalline power, readily soluble in water, slightly bitter, sensitive to light, and its mp is from 246 to 252 ºC. PPQ structure is shown in Fig. 2 [14].

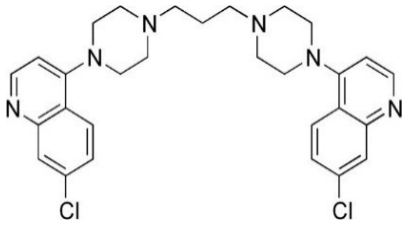

Figure 1: ATS structure.

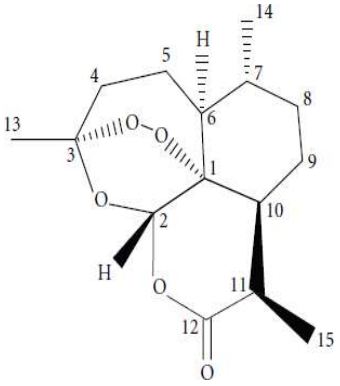

Figure 2: PPQ structure.

The aim of this study was to investigate ATK mains components (ATS and PPQ) IE(%) on A36 MS corrosion surface active sites, ascertaining its adsorption mechanism, Td and kinetic properties, using computational and electrochemical methods.

Materials and methods

Metal treatment and inhibitor preparation

The drug (an anti-malarial), sold under the trade name Artequick®, was obtained from Peaceland Pharmaceutical Shop, Calabar-Nigeria, and used without further purification, at a ratio of 1:6. ATK was weighed, powdered to fine particles size. and dissolved in a 1000 mL volumetric flask with 1 M HCl. The solution was filtered after 24 h, and different Ct of ATK (150, 250, 500, 600 and 750 ppm) were prepared for the corrosion test.

Tests were performed on A36 MS coupons with the following composition by wt%: 98.35 Fe, 1.03 Mn, 0.04 P, 0.28 Si, 0.05 S and 0.25 C. MS was obtained from a heavy duty shop in Calabar, Nigeria. The MS coupons were resized to dimensions of 2 x 0.08 x 4 cm, mechanically ground with 220, 800 and 1200 emery grade paper (using a UNIPOL-820 metallographic polishing machine), washed in distilled water, degreased in ethanol, rinsed in acetone, air dried, and then stored in a desiccator.

Gravimetric technique

CR of MS and IE(%) of ATK were tested by the WL method, in which different inhibitor Ct were placed in a 100 mL volumetric flask. The treated MS coupons were immersed by suspension in HCl. Initial IT was taken, and, after every 1 h, MS was removed, washed, degreased, rinsed, air dried, and then weighed using an ADAM PGW 253e electronic digital balance. This process continued for 6 h. Data generated from WL experiment were used to calculate CR and θ of MS, and IE(%) of ATK, using Eqs. 1 and 2.

$$\theta = \frac{WL_0 - WL_i}{WL_0} \quad (1)$$

$$IE\% = \frac{WL_0 - WL_i}{WL_0} \times 100 \quad (2)$$

where WL_0 and WL_i are WL for MS in 1 M HCl without and with ATK, respectively.

Tm technique

The same WL method was adopted here, except that the beakers were immersed in a Tm water bath (MEMMERT WNB-14), at regulated T of 298, 308, 318 and 333 K. After 60 min, MS was removed, washed with fast flowing distilled water, degreased with ethanol, rinsed in acetone and air-dried, before weighing. The same experiment was conducted with ATK, at Ct of 150, 250, 500, 600 and 750 ppm. Data generated from the trial were used to obtain CR and θ of MS, and IE(%) of ATK, as shown in Eqs. 3 and 4.

$$\theta = \frac{J_0 - J_i}{J_0} \quad (3)$$

$$IE\% = \frac{WL_0 - WL_i}{WL_0} \times 100 \quad (4)$$

where J_0 and J_i are CR, for MS in 1 M HCl without and with ATK, respectively.

EIS technique

EIS test was carried out at 303 K, in a three-electrode cell, using a Gamry 600 potentiostat/galvanostat, coupled with Gamry EIS300 framework. Echem Analyst software was used for data analyzing and fitting. The frequency range was from 100 kHz to 0.01 Hz, and AC signal amplitude was 10 mV. A Pt electrode was used as CE, SCE was used as RE and the WE was a MS exposed surface of 1 cm^2. Measurements were performed in an aerated solution, after 30 min (1800 s) IT in the test solution, at ambient T, in order to attain a steady state OCP. Nyquist plots derived in ATK absence and presence were used to obtain some useful kinetic parameters, including R_{ct}. IE(%) of ATK was calculated from its R_{ct}, according to Eq. 5.

$$IE(\%) = \frac{R_{cti} - R_{ct0}}{R_{cti}} \times 100 \quad (5)$$

where R_{ct0} and R_{cti} represent R_{ct} without and with ATK, respectively.

PDP technique

PDP tests were performed at 303 K, using a potentiostat, and data were analyzed using Echem Analyst. PDP curves were measured at a SR of 0.5 mV/s, from -0.25 to +0.25 V vs SCE. β_a and β_c, for MS dissolution in 1 M HCl, with and without ATK, were recorded. Their segments were extrapolated from the plots, which gave useful Td parameters. I_{corr} was used to calculate IE(%) of ATK, according to Eq. 6.

$$IE(\%) = \left[1 - \frac{I^0_{corr}}{I^i_{corr}}\right] \text{x } 100 \quad (6)$$

where I^0_{corr} and I^i_{corr} represent I_{corr} obtained without and with ATK, respectively.

SEM

SEM, model number JSM-5600 LV, from Tokyo, Japan, was used to produce micrographs of MS coupons immersed in 1 M HCl without and with ATK. Selected coupons were retrieved from the test solution (containing 750 ppm ATK, at room T), after 168 h IT. Each sample was mounted on a metal stub, and sputtered with gold, in order to make it conductive. Scanned micrographs were taken at an accelerating V of 2 and 15 kV.

Computational details

This study was performed using $DMol^3$ code of Material Studio software (BIOVIA, USA). Herein, ATS and PPQ were sketched, H molecules were adjusted, and the compounds were cleaned using a sketch tool available in the material visualizer. Sketched ATS and PPQ were enhanced using geometry optimization, in order to relax the atoms positions, and try to find the best bond angle and length. ATK geometry calculations were done in the gas phase, using medium SCF tolerance. DFT optimization involved GGA, with PBE function, and the double numerical basis set, with d-functions on H atoms (DND), and the basis file set to 4.4. The convergence tolerance energy was set to 2.0e-5 Ha or 5.4e-4 Ev, with maximum force of 0.004 Ha/Å, and maximum displacement of 0.005 Å. The iteration was set at a maximum of 100, using a max step size of 0.3 Å. No symmetry was used during optimization. The surface was cleaved using a {1 1 1} plane on the (h k l)

plane, respectively. Thereafter, the surface fractional thickness was increased to 4, which is equivalent to 9.352 Å. The vacuum slab crystal was built with vacuum thickness set to 20 Å, with orientation at C. The lattice maximum range for A, B and C was set to 4, 4 and 1, respectively. The super cell was created (the lower two layers were constrained) with the maximum range parameters. The bond was monitored for all elements, with a length tolerance from 0.6 to 1.344, and the lattice style was left unchanged. It is noteworthy that the lattice lengths used were 16.5138 (A), 16.5311 (B) and 26.9627 Å (C). The bond angle was 90 °, for α and β, and 60.0566 ° for γ. The lattice type used was 3D triclinic. Absolute χ, η, μ, σ, ω and δ were calculated using the output generated from E_{HOMO} and E_{LUMO}, with IP and EA, according to Eqs. 7-11.

$$\chi = \frac{IP+E}{2} \quad (7)$$

$$\eta = \frac{IP- EA}{2} \quad (8)$$

$$\sigma = \frac{1}{\eta} \quad (9)$$

$$\omega = \frac{\chi 2}{2\eta} \quad (10)$$

$$\delta = \frac{1}{\omega} \quad (11)$$

Results and discussion

Gravimetric (WL) results

Table 1 shows values obtained from WL data analysis. The results show that MS corrosion was strongly inhibited by ATK, of which higher IE(%) was 90.2%. MS corrosion was inhibited through ATK molecules adsorption onto its surface, which arose from their hetero-atoms and structural positioning, as earlier reported by [3, 15]. This was also attributed to Fe (a transition metal) higher percentage, which allowed for variable oxidation states and formation of a stronger metal-ligand complex [2, 15-16]. Electrons bonding and ease of transfer between MS and ATK molecules gave rise to their higher stability through adsorption onto the alloy surface. This optimized CI of MS by ATK [6, 9, 18]. CR of MS was lower in the HCl solution with ATK (19.3 mg/cm^2/h) than in that without it (197.6 mg/cm^2/h), especially with higher inhibitor Ct. This indicates an initial disturbance of HCl at its interface with MS, in ATK absence. HCl removed loosely held atoms from the MS surface, and caused anodic tendency for oxidation and subsequent corrosion [18-20].

Table 1: CR and θ of MS, and IE(%) of ATK, in 1 M HCl.

Ct (ppm)	CR (mg/cm^2/h)	θ	IE(%)
Blank	197.62	-	-
150	98.76	0.50	50.0
250	65.85	0.67	66.7
500	55.59	0.72	71.9
600	33.34	0.83	83.1
750	19.31	0.90	90.2

Tm analysis results

In response to ΔH effect on ATK viability, following its IE(%) values in WL measurements for MS, Tm data were obtained for the inhibitor, as shown in Table 2. The results showed ATK physical nature of adsorption. ATK lower IE(%), with high T, as shown by CR of MS in Table 2, does not only indicate a physical adsorption process, but also explains the loosely bounded inhibitor molecules elimination, due to heat agitation. Similar results were reported by [15]. The desorption process was not too significant, since, even at 333 K, IE(%) of ATK was 70.8%, as against 81.1%, at 298 K. This shows that, although ATK protected the MS surface better at higher T, it still acted at lower ones, which was due to the inhibitor molecules stronger adsorption onto the alloy [21-22]. The results are in agreement with those of WL.

Table 2: Tm data for MS corrosion and θ in 1 M HCl without and with ATK in different Ct, and its IE(%).

Ct (ppm)	CR (mg/cm²/min)				θ				IE(%)			
T (K)	298	308	318	333	298	308	318	333	298	308	318	333
Blank	87.73	100.17	113.11	128.57	-	-	-	-	-	-	-	-
150	64.05	75.23	85.06	99.26	0.27	0.25	0.25	0.23	27.0	24.9	24.8	22.8
250	54.74	63.51	74.43	87.30	0.38	0.37	0.34	0.32	37.6	36.6	34.2	32.1
500	46.15	53.79	62.32	73.03	0.47	0.46	0.45	0.43	47.4	46.3	44.9	43.2
600	28.60	33.26	39.82	54.00	0.67	0.67	0.65	0.58	67.4	66.8	64.8	58.0
750	16.58	21.33	29.64	37.54	0.81	0.79	0.74	0.71	81.1	78.7	73.8	70.8

Electrochemical results (EIS and PDP)

Nyquist plots and its corresponding equivalent circuit cell diagram are shown in Figs. 3 and 4, respectively.

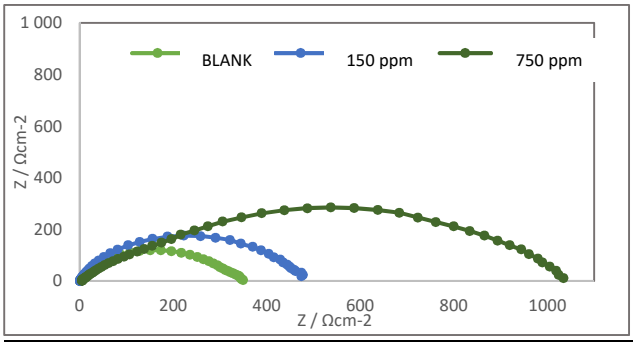

Figure 3: EIS for MS in 1 M HCl without and with ATK.

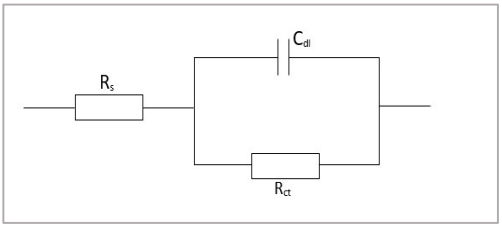

Figure 4: Equivalent circuit cell diagram for EIS.

High frequency loops with corresponding increased semicircles were obtained, which indicates stronger CI of ATK with higher Ct [4, 18, 23-24]. C_{dl} and IE(%) of ATK were determined from Eqs. 12-14 [20] (Table 3).

$$C_{dl} = \frac{1}{\omega Z''} \quad (12)$$

where Z" is impedance imaginary component and ω is angular frequency. Hence:

$$C_{dl} = \frac{1}{2\pi f_{max} Z''} \quad (13)$$

where f_{max} describe the semicircle max frequency and π is $\frac{22}{7}$.

$$\%\mathcal{E} = \frac{R_{ct}^{0} - R_{ct}^{i}}{\mathcal{R}_{ct}^{0}} \text{ x } 100 \quad (14)$$

where R_{ct}^{0} and R_{ct}^{i} are R_{ct} values in HCL solutions without and with ATK, respectively. From Table 3, R_{ct} data were found to increase with Ct, which confirmed retarded electrons transfer from the MS anodic sites trough ATK molecules adsorption onto the alloy surface. This also confirms MS lower CR and ATK higher IE(%), as earlier reported by [3, 15]. Decreased C_{dl} values were observed, which indicated separation, by ATK, of the electronic and electrolytic charges at the MS-HCl interface. This, in turn, led to CI of MS by ATK [19, 25-26].

Table 3: EIS parameters for MS in 1 M HCl without and with ATK, in varying C.

Ct (ppm)	R_s (Ω cm²)	R_{ct} (Ω /cm²)	Fmax (Hz)	C_{dl} (μF/cm²)	IE(%)
Blank	1.14	346	11.93	0.39	-
150	2.03	577	7.52	0.42	40.0
750	3.95	1153	3.75	0.28	70.0

Fig. 5 depicts Tafel plots.

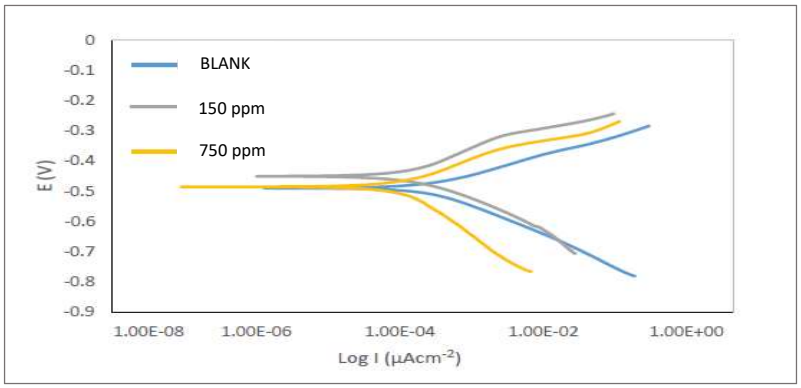

Figure 5: Tafel plots graphical representation of CI of MS and Al by ATK, in 1 M HCl.

The plots show divergence towards both anode and cathode sites, implying a mixed type phenomenon, as demonstrated in the works of [20, 26] (Table 4). However, i_{corr} values decreased while IE(%) increased. This implies that the current produced in the electrochemical cell decreased, while corrosion was occurring. This process is explained by ATK molecules strong adsorption onto MS

anodic sites, which slowed down electrons transfer from the anode to the cathode, with higher inhibitor Ct [27-30].

Table 4: Tafel plots theoretical analysis results for CI of MS by ATK, in 1 M HCl.

Ct (ppm)	β_a (V/decade)	β_c (V/decade)	I_{corr} (µA)	E_{corr} (mV)	C_R (mpy)	θ	IE($_{PDP}$%)	R_p (Ω)
Blank	0.0605	0.1030	312.2	-533.5	142.7	-	-	52.74
150	0.0814	0.1158	156.1	-450.4	48.7	0.50	50	132.88
750	0.0658	0.1831	62.4	-485.7	26.0	0.80	80	336.49

Quantum chemical calculations

E_{HOMO} and E_{LUMO} were employed to calculate global quantum chemical indices, using Eq. 15 [31]. In general, for a good CI with strong energy, E_{HOMO} value should be high, while E_{LUMO} and ΔE values should be low.

$$\Delta E = E_{LUMO} - E_{HOMO} \quad (15)$$

Fig. 6 shows FMO EDD of HOMO and LUMO, for ATS and PPQ.

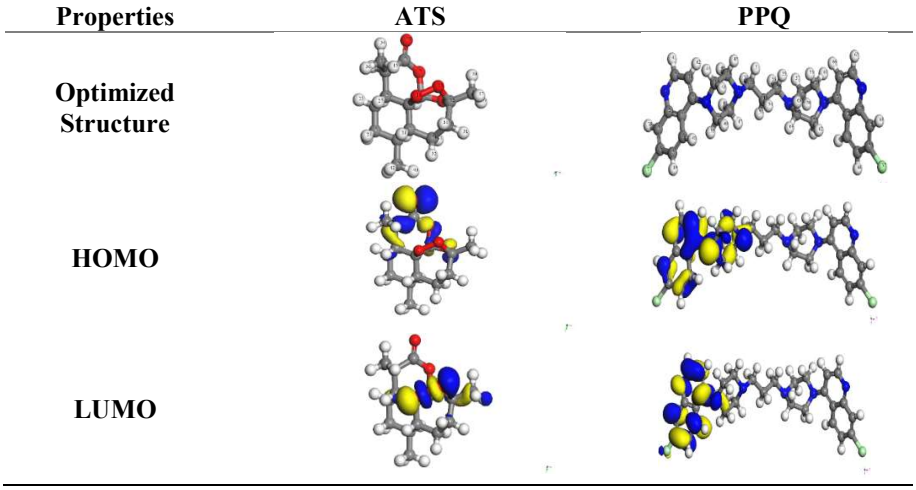

Figure 6: Optimized structure, HOMO and LUMO of ATS and PPQ compounds.

Fig. 6 shows that, for ATS, EDD at HOMO was strongly located on the heteroatoms, and in the carbonyl group (C=O). However, EDD at LUMO was on the O stereogenic centers and, therefore, IE(%) of ATS can be explained by the π electrons and free doublet of O heteroatoms, which favored electrons sharing between inhibitor and MS surface [32-34]. As for PPQ, EDD at HOMO was deeply located on the double bonds of the aromatic benzene ring and N heteroatoms. EDD at LUMO was located on the individual C atoms on the aromatic ring, heteroatoms and Cl atom as substituent. PPQ high IE(%) was linked to the donating power of π-electrons and heteroatoms in the aromatic ring, while the electron withdrawal properties were due to the halogen substituent (Cl) in the compound [31, 34-36].

Table 5 shows quantum chemical parameters for ATS and PPQ. IP values were obtained as E_{HOMO} negative values, using Eq. 16 [33]. Similarly, electrons

accepting ability, corresponding to EA, which was represented as E_{LUMO} negative value, was calculated from Eq. 17 [36].

$$IP = -E_{HOMO} \quad (16)$$

$$EA = -E_{LUMO} \quad (17)$$

ΔN was also calculated from Eqs. 18 and 19.

$$\Delta N = \frac{\varphi m - \chi i}{2(\eta m + \eta i)} \quad (18)$$

where φ_m is the work function for the Fe (110) surface (4.82 eV), χ_i represents absolute χ, and η_m and η_i represent global η for MS and inhibitors, respectively. $\Delta E_{b\text{-}d}$ was investigated using Eq. 19.

$$\Delta E_{b\text{-}d} = \frac{-\eta}{4} = \frac{(E_{HOMO} - E_{LUMO})}{8} \quad (19)$$

When η or $\Delta E_{b\text{-}d} < 0$, the latter, from the inhibitors to the metal surface, is energetically favored. From Table 5, $\Delta E_{b\text{-}d}$ for PPQ and ATS is -0.149 and -0.455, respectively. $\Delta E_{b\text{-}d}$ of PPQ was more negative than that of ATS, which means that the former was energetically favored [30-35]. The observed order for $\Delta E_{b\text{-}d}$ (PPQ > ATS) also suggests that PPQ is a better CI for MS than ATS. It was also seen that E_{HOMO} value of ATS was lower than that of PPQ, which means that the former is less prone to donate electrons to the MS surface. E_{LUMO} higher value for PPQ means it is less prone to accept electrons from MS. Therefore, PPQ is abler to donate electrons to MS, and it is a better inhibitor [34-36]. This can be verified from PPQ lower ΔE value (1.189 eV) than that of ATS (3.64 eV), which suggests that it has better polarization and CI properties [33-35].

Table 5: Quantum chemical parameters for ATS and PPQ.

Inhibitor	E_{HOMO}	E_{LUMO}	ΔE (eV)	IP (eV)	EA (eV)	χ (eV)	η (eV)	σ (eV)	ω (eV)	δ (eV)	ΔN	$\Delta E_{b\text{-}d}$
ATS	-5.35	-1.71	3.640	5.349	1.709	3.529	1.820	0.550	3.421	0.292	-0.1	-0.5
PPQ	-5.61	-4.42	1.189	5.605	4.416	5.011	0.595	1.681	21.10	0.047	-1.5	-0.2

Generally, particles with high ΔE are hard molecules, whereas those having low ΔE are referred to as soft ones [33-35]. Hard molecules are less reactive than soft ones. Thus, from Table 1, ATS is less reactive than PPQ, which makes the latter a better inhibitor than the former. However, ΔN was found to be less than 0 for both CI. This implies that they were able to transfer their electrons to MS, and that their IE(%) increased with enhanced electron-donating ability to the alloy surface [30, 32].

Local reactivity

In order to examine heteroatoms influence on IE(%), local reactivity was analyzed by evaluating Fukui indices (Fig. 7).

Three different types of Fukui functions, F(0), F^- and F^+ , were examined. Condensed Fukui functions were calculated by using the finite difference scheme from atoms MPA in the inhibitor molecules. Results obtained for the Fukui functions of the molecules atoms are shown on Fig. 6.

Obtained data revealed that, for ATS, C (12), C (10) and C (13) were most prone to attack by an electrophilic site. Thus, they likely would donate electrons in the order of C (12) >C (10) >C (13). O (16), O (15) and O (19) were most prone to attack by a nucleophile site. Therefore, they would likely accept electrons in the order of O (16) > O (15) > O (19) [29-33].

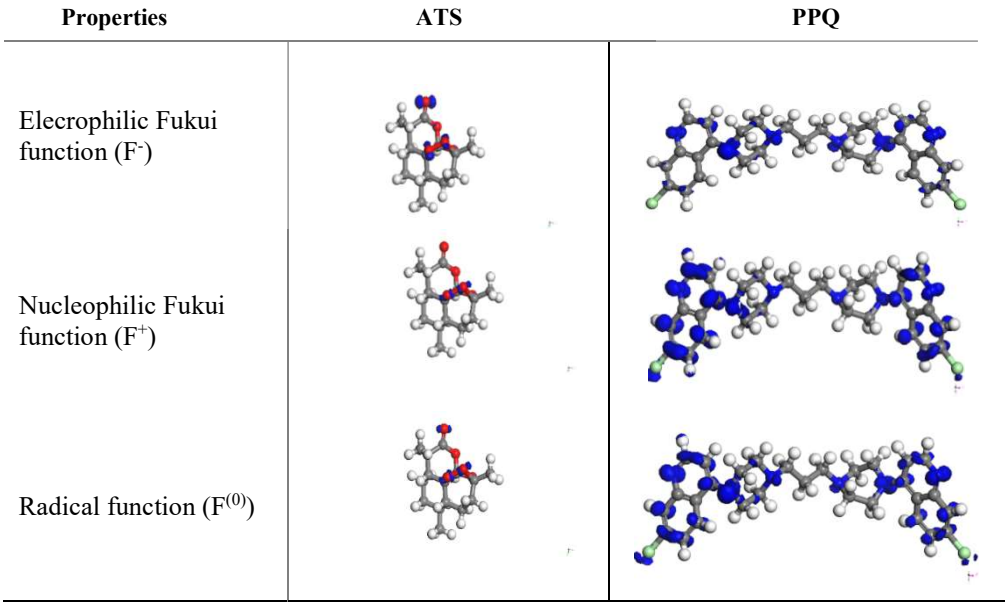

Figure 7: ATS and PPQ molecules f^-, f^+ and $f^{(0)}$ functions.

It is noteworthy that O (16)-O (15) > O (19) = C (9) (i.e., O to O single bond had stronger inductive effect than O to C double bond), for the nucleophilic site, while O (11) -C (12)-O (15) > C (10)-C (9) = O (19) > C (14)-C (13)-C (12). This was due to O, which pulled electrons from the nearby C atom, thus depleting it for the electrophilic charge site [35]. Fig. 6 also confirms that the surface was highly concentrated at O (16) and O (15) atoms, which acted as the most reactive site of ATS molecule for donor-acceptor interactions.

For PPQ, it was observed that Cl (7) had the highest positive atomic charge of 5.9, while C (23) had the highest negative charge of -1.2. Cl (7), Cl (37) and N (8) were most prone to nucleophilic attacks. Thus, they would likely accept electrons in the order of Cl (7) > Cl (37) > N (8), while C (23), C (13), C (25) and C (17) were most prone to attacks by the electrophilic site. Therefore, they would likely donate electrons in the order of C (23) > C (13) > C (25) ≡ C (17) [9, 12, 19-21].

From Fig. 6, it is clear that C (23)-N (24) ≥ C (13) –N (12) > C (25)-N (24) ≡ C (17)- N (12), majorly because of PPQ symmetry. The isosurfaces are highly concentrated on heteroatoms and C atoms in the phenyl ring. Thus, these were the most reactive sites of the molecule for donor-acceptor interactions [28-30, 35].

Td consideration

Eq. 20, which is the Arrhenius Eq., was deployed in E_a calculation.

$$k = Ae^{\frac{-Ea}{RT}} \tag{20}$$

where k is the rate and A is the collision factor, while other constants remain the same, as conventionally known. From Table 6, E_a values in HCl with ATK were

higher than in the blank, and also increased with higher Ct. This could be due to CR slowdown, due to ATK onto the MS surface [22-24], which agrees with WL results in Table 6, and shows its reliability as CI of MS [3-4, 9].

Table 6: Td data for MS corrosion in 1 M HCl without and with ATK, in varying C.

C_t (ppm)	E_a (kJ/mol^{-2})	R^{2*}	ΔH (kJ/mol^{-2})	- ΔS (kJ/mol^{-2})	R^{2**}
Blank	7.77	0.98	7.89	0.96	0.99
150	8.87	0.98	8.87	0.93	0.99
250	9.47	0.98	9.70	0.99	0.99
500	9.29	0.98	8.91	0.62	0.99
600	12.94	0.99	10.62	0.72	0.99
750	16.88	0.99	14.67	1.33	0.99

*R^2 for E_a; **R^2 for entropy change

An increase in the collisions led to higher CR. From values in Table 6, it was found that the pre-exponential factor increased with higher inhibitor C_t, which suggested a stronger ATK-MS reaction, due to molecular collision [4-6, 11]. The transition state Eq. for ΔH and ΔS_{ads} determination is as follows:

$$\ln\frac{k}{T} = -\frac{\Delta H_a}{R}\frac{1}{T} + \ln\frac{kB}{h} + \frac{\Delta S_a}{R} \quad (21)$$

where k is reaction rate, kB is Boltzman constant and h is Plank constant. Table 6 presents negative ΔS values, which imply an increased inhibition, due to the system reduced degree of randomness that allowed for ATK molecules stronger adsorption [3, 9,15-17]. ΔH_{ads} values lower than 80 kJ/mol^{-1} and positive represent a physical adsorption mechanism and an endothermic reaction, indicating bond breaking around the corrosion sites [5,17]. ΔG_{ads} values in Table 6 were negative and lower than -20 kJ/mol^{-1}, implying ATK physical adsorption, spontaneity of reaction and high stability [19-21]. These results showed strong agreement with gravimetric analysis.

Adsorption

Metallic CI by organic compounds is due to: either the inhibitor molecules adsorption onto the metal surface; or to the formation of a layer of an insoluble complex, such as the oxide film, on the metallic surface, which acts as a barrier between the metal and the aggressive medium [9-15]. The relationship between IE(%) and the bulk inhibitor C, at constant T, known as isotherm, gives an insight into the system adsorption process [2-5]. In order to investigate ATK adsorption mechanism, Langmuir's isotherm was employed and determined from Eq. 22-24, respectively.

$$\frac{C}{\theta} = \frac{1}{k} + C \quad (22)$$

Table 7 and Fig. 8 show that k values in the solution with ATK were lower than in that without it, which explains a physical adsorption phenomenon [12-17], confirming the results dependent from T, as already shown in Table 2. This result also indicates that stronger bonds between ATK and MS were possible, leading to high CI [12, 17, 22]. R^2 values showed that Langmuir's assumption was obeyed, which implies monolayer adsorption [1].

Table 7: Langmuir's isotherm and its Td parameters for MS in 1 M HCl, at various T.

T	298 K				308 K				318 K				333 K			
	k	-ΔG	slope	R^2	k	-ΔG	slope	R^2	k	-ΔG	slope	R^2	k	-ΔG	slope	R^2
Langmuir's	0.95	5.31	0.65	0.98	0.98	5.70	0.63	0.97	0.97	5.87	0.71	0.98	0.98	6.28	0.93	0.95

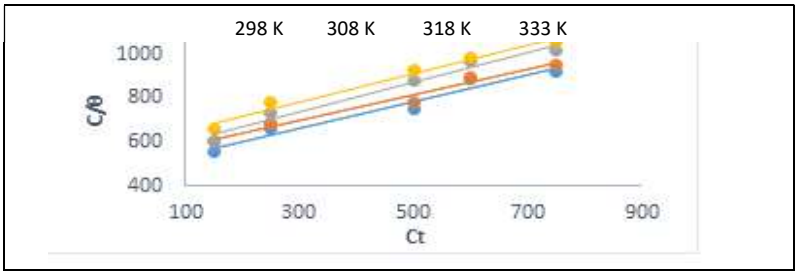

Figure 8: Langmuir's adsorption isotherm plots.

SEM

SEM micrographs of MS before and after immersion in 1 M HCl, without and with ATK, show that the inhibitor hindered corrosion. This was because the MS surface was less damaged (Fig. 9c) than that before and after immersion in 1 M HCl (Figs. 9a and b).

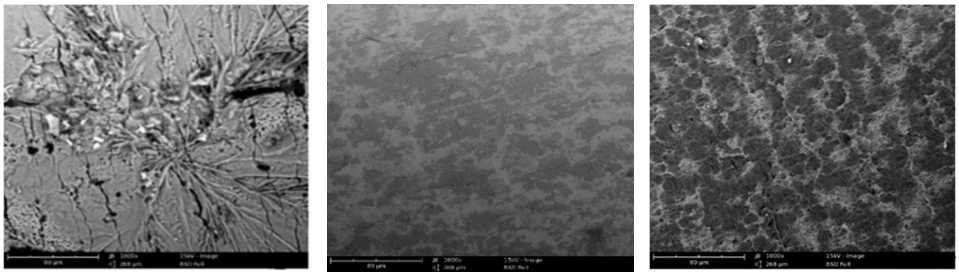

Figure 9: Micrographs of MS corrosion: **(a)** before immersion; **(b**) after immersion in 1 M HCl; and **(c)** after immersion in 1 M HCl + 750 ppm ATK.

This implies that there was no anodic dissolution and no possible cathodic HER, hence, less corrosion attack [33-34]. 750 ppm ATK in 1 M HCl formed a protective layer that filled up the corroded MS surface. It is clear that ATK inhibited MS corrosion, which agrees with results obtained from gravimetric and Tm studies.

Conclusions

It was concluded that ATK was a good alternative inhibitor (IE(%) = 90.2) against A36 MS corrosion caused by anodic dissolution and cathodic HER. PPQ presence in ATK improved its IE(%), which was due to the close ΔE and donating power of the π-electrons and heteroatoms in the aromatic ring, and to the electron withdrawal properties related to the halogen substituent (Cl) in the compound. Electrochemical results showed mixed type inhibition, with decreased C_{dl}, for effective adsorption. Simulation analyses showed ATK high IE(%),which confirms the experimental essay. SEM revealed a less damaged MS surface in ATK presence, which indicates the formation of an effective protective layer by the inhibitor on the metal surface.

Authors' contributions

B.U. Ugi: designed the research work; performed the experimental work; carried out data analysis and interpretation. **E. C. Omaliko**: was involved in the material and sample collection and preparation; performed the experimental work; carried out data analysis and interpretation. **M. E. Ikpi**: performed the experimental work. All authors read and reviewed the manuscript.

Abbreviations

Å: pertinent distances
AC: alternating current
ASTM: American Society for Testing Materials
ATS: artemisinin
ATK: Artequik® (mainly composed by artemisinin and piperaquine)
Ct: concentration
C_{dl}: double layer capacitance
CE: counter electrode
CI: corrosion inhibitor/inhibition
Cl: chlorine
CR: corrosion rate
CS: carbon steel
DFT: density functional theory
DNP: double numeric plus polarization
E_a: activation energy
EA: electron affinity
EDD: electron density distribution
E_{HOMO}: energy of the highest occupied molecular orbital
EIS: electrochemical impedance spectroscopy
E_{LUMO}: energy of the lowest unoccupied molecular orbital
EMF: electromotive force
FMO: Frontier molecular orbitals
GGA: generalized gradient approximation
Ha: Hartree
HCl: hydrochloric acid
HER: hydrogen evolution reaction
I_{corr}: corrosion current density
IE(%): inhibition efficiency
IP: ionization potential
IT: immersion time
IUPAC: International Union of Pure and Applied Chemistry
k: equilibrium constant
mp: melting point
MPA: Mulliken population analysis
MS: mild steel
OCP: open circuit potential
PBE: Perdew–Burke–Ernzerhof
Pc: phytocompounds
PDP: potentiodynamic polarization
PPQ: piperaquine

R^2: determination coefficient
R_{ct}: charge transfer resistance
RE: reference electrode
R_p: polarization resistance
SCE: saturated calomel electrode
SCF: self-consistent field
SEM: scanning electron microscopy
SR: scan rate
T: temperature
Td: thermodynamic
Tm: thermometric
WE: working electrode
WL: weight loss

Symbols definition

β_a: Tafel anodic slope
β_c: Tafel cathodic slope
δ: neucleophilicity
ΔE: energy gap
ΔE_{b-d}: back donation energy
ΔG_{ads}: adsorption free energy
ΔH: heat of adsorption
ΔH_{ads}: enthalpy of adsorption
ΔN: fraction of electrons transfer
ΔS_{ads}: entropy of adsorption
η: absolute hardness
θ: surface coverage
μ: chemical potential
σ: softness index
χ: absolute electronegativity
ω: electrophilicity index

References

1. Abdallah M, Gad EAM, Sobhi M et al. Performance of tramadol drug as a safe inhibitor for aluminum corrosion in 1.0 M HCl solution and understanding mechanism of inhibition using DFT. Egyp J Petrol. 2019;(28):173-181. http://doi.org./10.1016/j.ejpe.2019.02.003
2. Sharma S, Ganjoo R, Saha SK et al. Experimental and theoretical analysis of baclofen as a potential corrosion inhibitor for mild steel surface in HCl medium. J Adh Sci Technol. 2021;(1). https://doi.org/10.1080/01694243.2021.200230
3. Su P, Li L, Li W et al. Expired drug theophylline as potential corrosion inhibitor for 7075 aluminum alloy in 1 M NaOH solution. Int J Electrochem Sci. 2020;(15):1412-1425. http://doi.org./10.20964/2020.02.25
4. Tan J, Guo L, Wu D et al. Electrochemical and computational studies on the corrosion inhibition of mild steel by 1-Hexadecyl-3-methylimidazolium Bromide in HCl medium. Int J Electrochem Sci. 2020;(15):1893-1903 http://doi.org./10.20964/2020.03.36

5. Nkem BI, Ngozi JM, Lebe AN. The impact of tizanidine on E24 carbon steel corrosion inhibition in oil fied acidizing solution: experimental and quantum chemical studies. Emerg Mater. 2022;(3):196-212. http://doi.org./10.1007/s42247-022-00400-z
6. Cordelia UD, Nancy AM, Nkem BI et al. Adsorption and inhibition study of N-(5-methoxy-2-hydroxybenzylidene) isonicotinohydrazide Schiff base on copper corrosion in 3.5% NaCl. Egyp J Petrol. 2022;(31):31-37. https://doi.org/10.1016/j.ejpe.2022.05.001
7. Ameh PO, Eddy NO. Experimental and computational chemistry studies on the inhibition efficiency of phthalic acid (PHA) for the corrosion of aluminum in hydrochloric and tetraoxosulphate (VI) acids. Protec Met Phy Chem Surf. 2018;(2):1-13. http://doi.org./10.1134/S2070205118060035
8. Bharatiya U, Gal P, Agrawal A et al. Effect of corrosion on crude oil and natural gas pipeline with emphasis on prevention by ecofriendly corrosion inhibitors: a comprehensive review. J Bio-Tribo Corros. 2019;(5):35. http://doi.org./10.1007/s40735-019-0225-9
9. Agwamba EC, Udoikono AD, Hitler L et al. Synthesis, characterization, DFT studies, and molecular modeling of azo dye derivatives as potential candidate for trypanosomiasis treatment. Chem Phys Impact. 2022;(4):100076. http://doi.org./10.1016/chphi.2022.100076
10. Bhuvaneswari M, Santhakumari R, Usha C et al. Synthesis, growth, structural, Spectroscopic, optical, Thermal, DFT, HOMO–LUMO, MEP, NBO analysis, and Thermodynamic properties of vanillin isonicotinic hydrazide single crystal. J Mol Struct. 2021;(4):130856. http://doi.org./10.1016/j.molstruc.2021.130856
11. Boumhara K, Harhar H, Tabyaoui M et al. Corrosion inhibition of mild steel in 0.5 M H_2SO_4 solution by *Artemisia herba-alba* oil. J Bio-Tribo Corr. 2019;(5):1-8. http://doi.org./10.1007/s40735-018-0202-8
12. Dagdag O, El Harfi A, Cherkaoui O et al. Rheological, electrochemical, surface, DFT and molecular dynamics simulation studies on the anticorrosive properties of new epoxy monomer compound for steel in 1 M HCl solution. RSC Adv. 2019;(9):4454-4462. http://doi.org./10.1039/c8ra09446b
13. Diki NYS, Coulibaly NH, Kambire O et al. Experimental and theoretical investigations on copper corrosion inhibition by cefixime drug in 1 M HNO_3 solution. J Mater Sci Chem Eng. 2021;(9). http://doi.org./10.4236/msce.2021.95002
14. Dimakis N, Salas I, Gonzalez L et al. Li and Na adsorption on graphene and graphene oxide examined by density functional theory, quantum theory of atoms in molecules, and electron localization function. Molecules. 2019;(24):754. http://doi.org./10.3390/molecules24040754
15. Ebenso EE, Verma C, Olasunkanmi LO et al. Molecular modelling of compounds used for corrosion inhibition studies: a review. Phys Chem. 2021;(23):19987- 20027. http://doi.org./10.1039/D1CP00244A
16. Solomon MM, Umorena SA, Quraishia MA et al. Effect of akyl chain length, flow, and temperature on the corrosion inhibition 1 of carbon 2 steel in a simulated acidizing environment by an imidazoline-based inhibitor. J Petrol Sci Eng. 2020;(2):1-39. http://doi.org./10.1016/j.petrol.2019/106801
17. Fajobi MA, Fayomi OSI, Akande IG et al. Inhibitive Performance of Ibuprofen Drug on Mild Steel in 0.5 M of H_2SO_4 Acid. J Bio-Tribo Corros. 2019;(5):1-5. http://doi.org./10.1007/s40735-019-0271-3

18. Fouda AES, El-Askalany AH, Molouk AFS. Experimental and computational chemical studies on the corrosion inhibitive properties of carbonitrile compounds for carbon steel in aqueous solution. Sci Rep. 2021;(11):67-79. http://doi.org./10.1038/s41598-021-00701-z
19. Geerlings P, Chamorro E, Chattaraj PK et al. Conceptual density functional theory: status, prospects, issues. Theor Chem Account. 2020;(139):36. http://doi.org./10.1007/s00214-020-2546-7
20. Hsissou R, Abbout S, Seghiri R et al. Evaluation of corrosion inhibition performance of phosphorus polymer for carbon steel in [1 M] HCl: Computational studies (DFT, MC and MD simulations). J Mater Res Technol. 2020:(9):2691-2703. http://doi.org./10.1016/j.jmrt.2020.01.002
21. Ammouchi N, Allal H, Belhocine Y et al. DFT computations and molecular dynamics investigations on conformers of some pyrazinamide derivatives as corrosion inhibitors for aluminum. J Mol Liq. 2020;(300):112309. http://doi.org./10.1016/j.molliq.2019.112309
22. Bashir S, Sharma V, Kumar S et al. Inhibition performances of Nicotinamide against aluminum corrosion in an acidic medium. Port Electrochim Acta. 2020;(38):107-123. http://doi.org./10.4152/pea.202002107
23. Bai Y, Sui H, Liu X et al. Effects of the N, O, and S heteroatoms on the adsorption and desorption of asphaltenes on silica surface: a molecular dynamics simulation. Fuel. 2019;(240):252-261. http://doi.org./ 10.1061/j.fuel.2018.11.135
24. Jiajun FU, Su-ning L, Wang Y. Computational and electrochemical studies of some amino acid compounds as corrosion inhibitors for mild steel in hydrochloric acid solution. J Mater Sci. 2020;(45):6255-6265. http://doi.org./10.1007/s10853-010-4720-0
25. Joshi BD, Thakur G, Chaudhary MK. Molecular structure, homo-lumo and vibrational analysis of ergoline by density functional theory. Sci World 2021;(14):21-30. http://doi.org./10.3126/sw.v14i14.34978
26. Liu Q, Song Z, Han H et al. A novel green reinforcement corrosion inhibitor extracted from waste *Platanus acerifolia* leaves. Con Build Mat. 2020;(260):119695. http://doi.org./10.1016/j.conbuildmat.2020.119695
27. Majda MT, Ramezanzadeh M, Ramezanzadeh B et al. Production of an environmentally stable anti-corrosion film based on Esfand seed extract molecules-metal cations: Integrated experimental and computer modeling approaches. J Hazard Mat. 2020;(382):1-16. http://doi.org./10.1016/j.hazmat.20192019.121029
28. Onyeachu IB, Abdel-Azeim S, Chauhan DS et al. Electrochemical and Computational insights on the application of expired Metformin drug as a novel inhibitor for the sweet corrosion of C1018 steel. ACS Omega 2021;(6):65-76. http://doi.org./10.1021/acsomega.0c03364
29. Padash R, Sajadi GS, Jafari AH et al. Corrosion control of aluminum in the solutions of NaCl, HCl and NaOH using 2, 6-dimethylpyridine inhibitor: Experimental and DFT insights. Mat Chem Phys. 2020;(244):122681. http://doi.org./10.1016/j.matchemphys.2020.122681
30. Rbaa M, Ouakki M, Galai M, et al. Simple preparation and characterization of novel 8-Hydroxyquinoline derivatives as effective acid corrosion inhibitor for mild steel: Experimental and theoretical studies. Col Surf A: Physicochem Eng Aspects. 2020;(602):125094. http://doi.org./10.1016/j.colsurfa.2020.125094
31. Thanh LT, Vu NSH, Binh PMQ et al. Combined experimental and computation studies on corrosion inhibition of *Houttuynia cordata* leaf extract for steel in HCl medium. J Mol Liq. 2020;(315):113787 http://doi.org./10.1016/j.molliq.2020.113787

32. Ugi BU, Obeten ME, Bassey VM, et al. Adsorption and inhibition analysis of aconitine and tubocurarine alkaloids as eco-friendly inhibitors of pitting corrosion in ASTM – A47 low carbon steel in HCl acid environment. Indones J Chem. 2022;(22):1-16. http://doi.org./10.22146/ijc.56745
33. Xi J, Liu C, Morgan D et al. An Unexpected Role of H During SiC Corrosion in Water. The J Phys Chem C. 2020;(124):9394-9400. http://doi.org./10.1021/acs.jpcc.0c02027
34. Zaher A, Chaouiki A, Salghi R et al. Inhibition of mild steel corrosion in 1M hydrochloric medium by the methanolic extract of *Ammi visnaga* l. Lam seeds. Hindawi Int J Corr. 2020;(1):1-10. http://doi.org./10.1155/2020/9764206
35. Ikpi ME, Abeng FE, Udowo VM. Computational studies of the corrosion inhibition potentials of Quercetin and Coumarin. Arc Org Inorg Chem Sci. 2018;(2):17-29. http://doi.org./10.32474/AOICS.2018.02.000133
36. El-Monem MA, Shaban MM, Khalil MMH. Synthesis, Characterization and computational chemical study of Aliphatic Tricationic surfactants for metallic equipment in oil fields. ACS Omega. 2020;(5):26626-26639. http://doi.org./10.1021/acsomega.0c03432
37. Erazua EA, Adeleke BB. A computational study of quinolone derivatives as corrosion inhibitors for mild steel. J Appl Sci Environ Manag. 2019;(23):1819-1824. http://doi.org./10.4314/jasem.v23i10.8
38. Erteeb MA, Ali-Shattle EE, Khalil SM et al. Computational studies (DFT) and PM3 theories on thiophene oligomers as corrosion inhibitors for iron. Americ J Chem. 2021;(11):1- 7 http://doi.org./10.5923/j.chemistry.20211101.01